Available online at www.sciencedirect.com

ScienceDirect

Acta Materialia 77 (2014) 191–199

Acta MATERIALIA

www.elsevier.com/locate/actamat

The kinetics of the ω to α phase transformation in Zr, Ti: Analysis of data from shock-recovered samples and atomistic simulations

Hongxiang Zong [a,b], Turab Lookman [b,*], Xiangdong Ding [a], Cristiano Nisoli [b], Don Brown [c], Stephen R. Niezgoda [c], Sun Jun [a]

[a] State Key Laboratory for Mechanical Behavior of Materials, Xi'an Jiaotong University, Xi'an 710049, China
[b] Theoretical Division, Los Alamos National Laboratory, Los Alamos, NM 87545, USA
[c] Materials Science and Technology Division, Los Alamos National Laboratory, Los Alamos, NM 87545, USA

Received 11 April 2014; accepted 23 May 2014

Abstract

An open question in the kinetics of martensitic transformation is the microscopic mechanism responsible for the evolution of a new phase. We have analyzed data from shocked recovered samples that monitor the volume fraction of the ω phase in α-Zr as a function of time under isothermal conditions in the temperature range 430–545 K. Our results show that the effective activation energy strongly depends on the peak pressures of shock compression. In addition, we confirm that the orientation relationship in Zr for this reverse transformation is consistent with the original suggestion by Silcock in Ti for a direct $\alpha \rightarrow \omega$ martensitic transition. Combined with large-scale molecular dynamics simulations, we find that the difference in the effective activation energy, which is related to the nature of the isothermal kinetics, is controlled by heterogeneous nucleation from defects in the microstructure.

Keywords: Activation energy; Martensitic transition; Zirconium; Phase transformation kinetics

1. Introduction

The kinetics of phase transformations play a crucial role in determining how the volume fraction of martensite depends on temperature and time [1–3]. Two cases can be distinguished. For an athermal martensitic transformation (MT) which is nonthermally activated, the volume fraction of product phase depends on temperature, and is essentially independent of time [4]. The transformation proceeds by the triggering of martensite formation as the temperature is lowered. For an isothermal MT (thermally activated), there is a critical temperature (T_0) below which martensite formation can be triggered as a function of time [5]. This type of transformation can be hindered by rapid cooling, but then occurs gradually with time by the formation of increasing volume fractions of martensite if the temperature is kept constant below T_0. In addition, the isothermal MT behavior can be described by a time–temperature transformation (TTT) curve, similar to that used for diffusional phase transformations (such as crystallization, second phase precipitation).

Here we consider the pressure driven martensitic α (hexagonal close-packed) to ω (simple hexagonal) transformation in zirconium and titanium, which is thought to be a combination of isothermal–athermal processes [6–8], with significant implications in engineering and medicine [9]. Analysis of quasi-static pressure data (5–9 GPa) based on resistivity measurements suggest that the kinetics of the $\alpha \rightarrow \omega$ transformation is of the isothermal MT type [6,10], and the time-dependent nature of the transformation indicates that there is an activation barrier of

* Corresponding author. Tel.: +1 505 665 0419.
E-mail address: txl@lanl.gov (T. Lookman).

http://dx.doi.org/10.1016/j.actamat.2014.05.049
1359-6454/

0.597 eV to spontaneous growth [11]. Further, it is found that the transformation rate increases rapidly with increase in pressure [10]. Two mechanisms have been suggested for the kinetics of this MT: (i) the transformation starts from quasi-static ω embryos created from the defects in the structure by a nucleation step. These embryos grow to critical size by a thermally activated process. A rapid increase in isothermal rate would result if somehow the critical radii of ω embryos decrease with increasing pressure [6]; and (ii) the kinetics of $\alpha \rightarrow \omega$ is a combination of an isothermal–athermal process. An increase in pressure can lead to a change from the isothermal MT to an athermal process, as which can occur under shock driven conditions (an adiabatic process) [11]. Therefore, studying the origin of the activation barrier for the $\alpha \rightarrow \omega$ transformation allows us to interpret possible mechanisms for the transformation kinetics.

In this work we study the kinetics of the reverse $\omega \rightarrow \alpha$ transformation in recovered samples of shocked Zr under isobaric–isothermal conditions. Specifically, we analyze data from measurements of the volume fraction change of the metastable ω phase in polycrystal Zr shocked samples upon isothermal annealing by employing in situ X-ray diffraction techniques. Our results for the reverse $\omega \rightarrow \alpha$ transformation show that the material shocked to a peak pressure of 10.5 GPa has a higher activation energy than specimens shocked to 8.0 GPa. Combined with large-scale molecular dynamics (MD) simulations, we analyze the experimental data and interpret this activation barrier difference as controlled by heterogeneous nucleation from defects (including the α–ω interfaces) in the material. In addition, we show that the crystal orientation relationship for the reverse $\omega \rightarrow \alpha$ transformation in Zr is consistent with the original suggestion by Silcock for the $\alpha \rightarrow \omega$ martensitic transition for Ti [12]. This finding is in agreement with interpretations of recent in situ high-pressure Deformation-DIA measurements on Zr polycrystal samples using similar X-ray techniques [13] that appear to show reversibility in this orientation relationship.

2. Methodology

2.1. Measurements on shock-recovered Zr samples

It is well known that Zr displays three phases as a function of pressure and temperature. At ambient conditions Zr stabilizes in the α phase, and under high pressure the α phase transforms into the ω phase. The $\alpha \rightarrow \omega$ transformation exhibits a very large hysteresis which results in the retention of the metastable high pressure ω phase on release to atmospheric pressure. The metastable ω phase can transform back to α phase on isothermal annealing of the specimens at a higher temperature, which provides a means to study the kinetics of the $\alpha \rightarrow \omega$ transformation at atmospheric pressure. The metastable ω phase can be obtained from α-Zr by high-pressure measurements using diamond anvil cells, shock compression or high-pressure torsion [6,14–15]. Here the initial metastable microstructure with different volume fractions of the retained ω phase was obtained via shock measurements at several peak pressures. These experiments and accompanying VISAR wave profiles for the specimens have been reported recently [16,17]. The high-purity samples had an average grain size of 15–20 μm, with a strong basal texture nearly aligned with the through thickness direction of the plate. The targets were impacted by 2.5 mm thick Zr flyer plates accelerated to velocities of either 640 or 835 m s^{-1}, resulting in peak compressive stresses of 8 or 10.5 GPa, respectively, on the Zr specimens. A high X-ray energy of 86 keV was utilized to penetrate into and probe the bulk of the material. Rietveld refinement of the observed diffraction patterns was completed to determine the α and ω volume fractions and lattice parameters; single peak fits were utilized to monitor specific grain orientations [18].

The volume fractions significantly depended on the peak stress of the plate impact experiment so that 82% and 63% volume fractions of the retained ω phase were obtained for the high and low peak pressure shocked samples, respectively. During the in situ annealing experiments, the temperature was held at five fixed temperatures in the range from 430 to 545 K, while diffraction images were recorded continuously. Previously reported in situ X-ray diffraction experiments increased the temperature of a given sample from room temperature (RT) to 600 K at a continuous rate for 3 K min^{-1}, while the volume fraction was monitored in a series of steps so that at each temperature the sample was allowed to relax until there was no further change in the measured intensity [16]. The stepwise loading has not been previously studied.

2.2. Simulation methods

To capture the microscopic mechanisms for the kinetics of the $\alpha \rightarrow \omega$ transformation, we investigate this problem at the atomic scale using MD simulations on Ti. Experimental studies on the $\alpha \rightarrow \omega$ transformation in Ti and Zr indicate that, as expected, the phase transformation behaviors are similar [6]. In addition, both are shuffle- (displacement) and shear-driven transformations. Moreover, a well tested potential for this transformation for MD simulations is available for Ti (unlike Zr), and we have previously used it to study anisotropic behavior in Ti under shock [19]. A spline-based MEAM potential was used to describe the phase transformation behavior, and this empirical potential is unique in describing the transformation between the α and ω phases in Ti [20]. The initial microstructures for our simulations were constructed by forming a mixture of α and ω phases with different volume fractions, analogous to the shock-recovered Zr samples in our experiment. Before measuring the transformation kinetics, the samples were thermally equilibrated at RT for 100 ps by using a Nosé–Hoover thermostat [21] within an NPT ensemble, where N, P, and T denote the number of atoms, hydrostatic pressure and absolute temperature, respectively. The

samples were then isothermally annealed at a fixed temperature above T_0. A bond-order parameter introduced by Ackland and Jones [22] is used to identify the local structure, as well as the volume fraction of the α and ω phases. The atomic simulations were carried out using the LAMMPS code [23] and the atomic configurations visualized by ATOMEYE [24].

3. Results and discussion

3.1. Isothermal nature of the ω to α transformation for shock-recovered Zr samples

To assess the kinetic nature of the $\omega \rightarrow \alpha$ MT, the volume fraction, η, of the retained ω phase is collected at various times and temperatures between 443 and 518 K to determine the temperature-dependent reaction rates (as shown in Fig. 1). We then used a Poisson distribution or a modified Kohlrausch–Williams–Watts relation [25] to fit the time-dependent volume fraction $\eta(t)$. For a solid-state phase transformation occurring upon isothermal annealing, $\eta(t)$ can be expressed as

$$\eta(t) \propto t^{-\alpha} \cdot \exp\left(-\left(\frac{t}{\tau(T)}\right)^{\beta}\right) \tag{1}$$

where the prefactor $t^{-\alpha}$ is associated with the non-thermally activated events. T is the absolute temperature and τ is the relaxation time. At $t = \tau$, $\eta = \exp(-1) \approx 0.37$. Thus, the relaxation time is defined as the time required for 37% of the transformation to take place.

In order to reduce the dimensionality of the fitting parameters, we define a normalized transformation rate as

$$\eta'(t) = \dot{\eta}(t)/\dot{\eta}(0) \tag{2}$$

Thus, the normalized transformation rate-controlling equation is given by

$$\eta'(t) = t^{-\alpha} \cdot \exp\left(-\left(\frac{t}{\tau(T)}\right)^{\beta}\right) \tag{3}$$

As shown in Fig. 3, a series of data sets for discrete temperatures are fitted to Eq. (3). The left panels show the data collected from isothermal annealing results of the 8 GPa pressure-shocked samples, while the normalized transformation rates of the 10.5 GPa-shocked samples are shown in the right panels. The η'–t plot Fig. 2 is typical for thermally activated processes where the transformation rates initially decrease significantly by factors of 5–10 as the transformation progresses for a short time, then become much slower in the later stages. The parameters α and β are given in Table 1 and, with the prefactor $t^{-\alpha}$ close to 1, the data indicates that the kinetics is dominated by a stretched exponential, slow relaxation process in which the exponent β is close to 0.5, indicative of glassy-like behavior due to frustration or pinning effects [26–28] during transformation below 503 K. The relaxation becomes faster at a temperature of 513 K, and the trend at higher temperatures is towards an exponential decay. Typical relaxation times, τ, for the two types of shocked specimens with 63% and 82% volume fractions of retained ω phase at the selected temperatures are shown in Fig. 3. The relaxation times decrease rapidly with increasing temperature for both cases. The temperature dependence of the relaxation time may be assumed to be dominated by thermal activation so that the activation energies (ΔE) can be extracted, i.e. the time for a given fraction of transformed phase, η, is given by

$$\ln(t_\eta(T)) = b_0 + \frac{\Delta E}{k_B T} \tag{4}$$

where b_0 is a constant and k_B is the Boltzmann constant. All our discussion is confined to $t_\eta = \tau$. Interestingly, we find that the activation energy, given from the slope of the curve, is very nearly independent of temperature in the temperature range investigated (443–518 K). Moreover, we find that the activation barrier increases with the peak pressure for metastable microstructure from shocked Zr. Specifically, the 10.5 GPa-shocked microstructure presents an energy barrier to the reverse transformation of 1.73 eV,

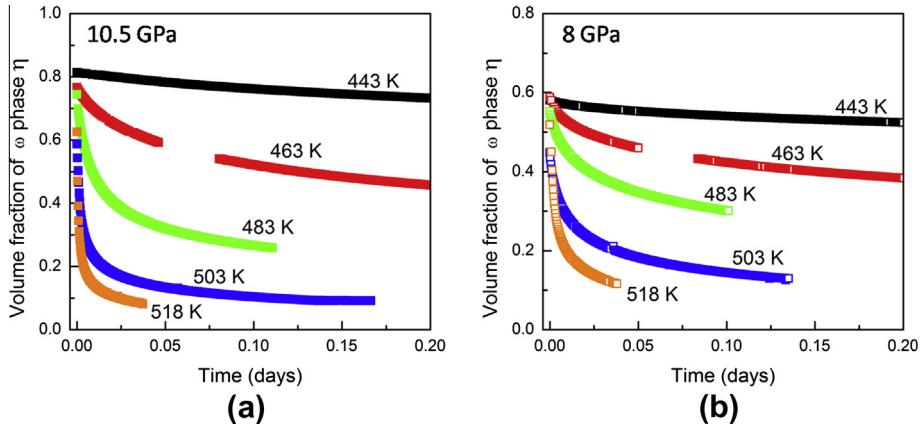

Fig. 1. The volume fraction of ω phase for two shocked samples upon isothermal annealing via in situ X-ray diffraction techniques. (a) Data for shocked sample at a peak pressure of 10.5 GPa; (b) data for the sample at 8 GPa.

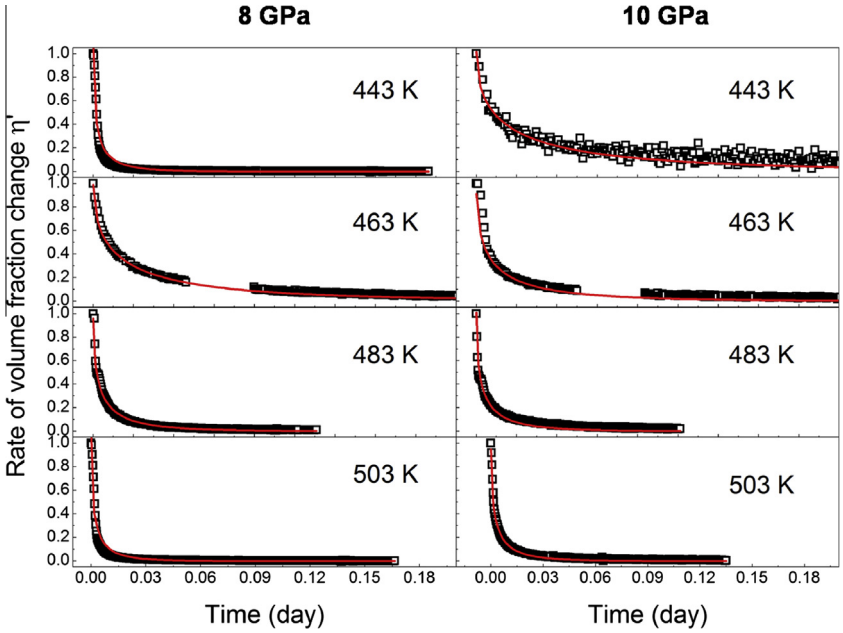

Fig. 2. The reduced transformation rate of ω phase for two shocked samples upon isothermal annealing. The left panels shows the isothermal behavior for the high-velocity-shocked samples at five temperatures, while the transformation rates of the low-pressure-shocked samples are shown in the right panels.

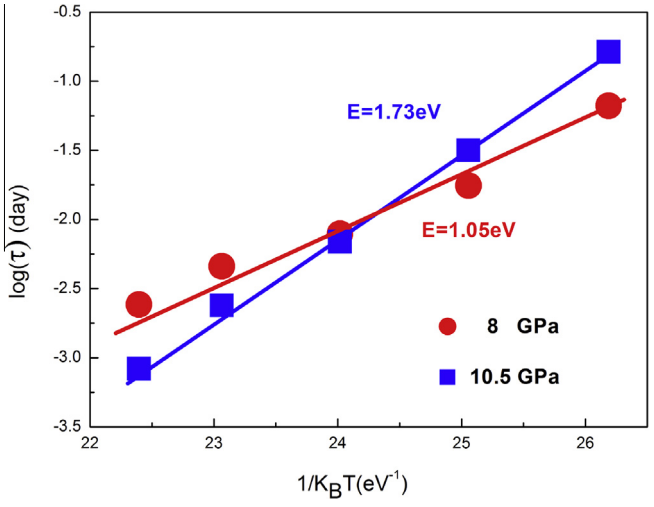

Fig. 3. The effective activation energy for the $\omega \rightarrow \alpha$ transformation. The logarithm of relaxation time $\log(\tau)$ vs. the inverse absolute transformation temperature, $1/k_BT$, from the analysis of the in situ data on heating the shock-recovered metastable samples at a fixed temperature. The activation barrier is almost independent of temperature, but is higher for the higher peak stress and ω volume fraction.

compared to 1.05 eV for the 8 GPa-shocked sample. Resistivity measurements gave an estimate of 0.597 eV for the energy barrier for the pressure-induced forward $\alpha \rightarrow \omega$ transformation. This barrier is also found to be independent of pressure in the range 5–12 GPa. Our barrier estimates from shock measurements based on isothermal heating for the reverse transformation are clearly higher that the forward measurements as a function of pressure at RT. Direct comparisons are difficult due to differing conditions; however, the trend is consistent with estimates

Table 1
The normalized rate of volume fraction of ω phase is fitted to the functional form $t^{-\alpha}\exp((t/\tau)^{\beta})$ for peak stresses of 8 and 10.5 GPa.

	Temperature				
	443 K	463 K	583 K	503 K	518 K
α (8.0 GPa)	0.0076	0.00404	0.0063	0.00364	0.00248
β (8.0 GPa)	0.54	0.54	0.54	0.54	0.8
α (10.5 GPa)	0.00335	0.000342	0.00411	0.0092	0.00118
β (10.5 GPa)	0.54	0.54	0.54	0.54	0.8

The very small value of the fitting parameter α indicates that we can neglect the power-law behavior in favor of the dominant slow kinetics given by the stretched exponential.

from ab initio calculations [29], and these estimates can potentially parametrize and therefore constrain free energy potentials for phase field and single crystal plasticity models.

3.2. Transformation mechanism for $\alpha \rightarrow \omega$ MT: reverse transformation by Silcock

The kinetics of MT are often associated with the transformation pathways or mechanisms, as these determine the nucleation barrier for a martensitic embryo and the propagation characteristics of the martensitic interface. Here we investigate the transformation mechanism for $\omega \rightarrow \alpha$ (reverse) upon heating. There are two commonly observed direct (i.e. without intermediate structures) transformation pathways in Zr, Ti for the $\alpha \rightarrow \omega$ transformation, namely, Silcock and TAO-1 [29]. The Silcock pathway is defined by the orientation relationship (OR) $\{1\bar{2}10\}_\alpha // \{0001\}_\omega, [1\bar{2}10]_\alpha // [0001]_\omega$ whereas TAO-1 is defined by $\{0001\}_\alpha // \{0\bar{1}11\}_\omega, [1\bar{2}10]_\alpha // [01\bar{1}1]_\omega$. The former was

conjectured on crystallographic grounds and the TAO-1 pathway, with lower energy, was predicted based on symmetry and ab initio calculations. However, it is the Silcock pathway which has invariably been observed experimentally in both Ti and Zr. It is accompanied by a coordinated set of atom shifts so that the displacements involve movements in the $[1\bar{2}10]$ direction with a magnitude of 0.74 Å and subsequently in the $[10\bar{1}0]$ direction with a magnitude 0.204 Å. The first displacement occurs in the same manner for three neighboring atoms and in the opposite direction for the next three, and so on. The second displacement occurs in the opposite sense for successive (0001) planes. This transforms the $(1\bar{2}10)_\alpha$ plane into the $(0001)_\omega$ plane, as shown in Fig. 4. These shifts are accompanied by a tensile strain ($e_2 = 0.05$) along $[10\bar{1}0]_\alpha$, as well as a compression strain ($e_3 = -0.05$) along the $[1\bar{2}10]_\alpha$ direction.

In situ synchrotron X-ray diffraction provides a means to infer ORs by monitoring dominant changes in intensity corresponding to different crystal orientations as a function of time or strain. Fig. 5(a) shows X-ray diffraction intensities from a sample shocked to 8 GPa peak pressure (black) and following subsequent continuous heating to 630 K (red). Fig. 5(b) shows the diffracted peak intensity of several crystal orientations (*hkl*) from both phases as a function of temperature during continuous heating of the 8 GPa peak stress sample. The ω or α single peak intensities are normalized to 1 to allow the data to be shown on a single scale. There is a small degree of crystal orientation dependence in the temperature at which peak intensities begin to evolve, as shown in Fig. 5(b). Below 470 K, the $(100)_\alpha$, $(002)_\alpha$ and $(110)_\alpha$ peak intensities are constant; the $(101)_\alpha$ and $(102)_\alpha$ peaks begin to increase slightly at temperatures below 470 K. All α peak intensities increase rapidly above 470 K. The $(110)_\omega$, $(112)_\omega$ and $(001)_\omega$ peak intensities begin to decrease slowly below 470 K. Above 470 K all ω peak intensities drop rapidly with increasing temperature. Now the most rapidly varying intensities, I, for the ω $\{\alpha\}$ single peaks (that is, $\frac{\partial I_\alpha}{\partial t} = -\frac{\partial I_\omega}{\partial t}$ during the transformation) are given by $(001)_\omega$ $\{(110)_\alpha\}$ from the temperature-dependent peak intensities. The correlation $C(f'_\alpha, f'_\omega) = \langle -\frac{\partial I_\alpha}{\partial t} \cdot \frac{\partial I_\omega}{\partial t} \rangle$ (units $\times 10^{-5}$) between the transformation rate of α and ω phase for the Silcock $(001)_\omega$ $\{(110)_\alpha\}$ is 2.37, compared to 0.97 for the $(111)_\omega$ $\{(002)_\alpha\}$TAO-1 mechanism. This is in accordance with the interpretation from recent high-pressure measurements for polycrystal Zr using deformation-DIA methods [13], which indicate that the Silcock relationship is obeyed for both the forward and reverse transformations.

3.3. Understanding the isothermal nature via atomistic simulations

3.3.1. MT kinetics of shocked Ti samples via MD simulations

In order to compare our findings from measurements to predictions, we studied the time evolution of the $\omega \rightarrow \alpha$ transformation by performing nonequilibrium molecular dynamics and large-scale equilibrium MD simulations. We performed shock simulations [19] starting with an ideal α structure, with the shock direction along the [0001] direction and with piston velocities of 750 and 900 m s^{-1}. These velocities correspond to peak pressures of 17.0 and 21.5 GPa, respectively. The shocked samples were then annealed at fixed temperatures from 600 to 1000 K, and the volume fraction of ω was calculated as a function of time. The annealing data from the MD simulations were then fitted to Eq. (3). The results obtained for the selected temperatures and piston velocities are shown in Fig. 6. Significant differences in the relaxation times can clearly be observed when varying the annealing temperature. In particular, the 900 m s^{-1} piston velocity shocked sample gives a higher activation barrier (independent of temperature) than the 750 m s^{-1} shocked sample. Our results for the dependence of relaxation time on the piston velocity or peak pressure from atomistic simulations follow the same trend as shown by the experimental results.

3.3.2. Atomic simulations of the isothermal annealing model

Despite much effort, the problem of adequately interpreting the nature of isothermal MT is far from clear

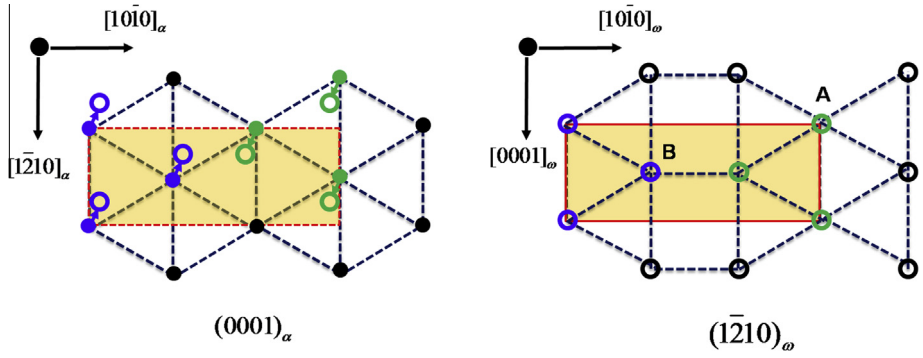

Fig. 4. The Silcock pathway for $\alpha \rightarrow \omega$ phase transformation, showing the shuffle or displacements of atoms from the $(0001)_\alpha$ to the $(1\bar{2}10)_\omega$. In each stacking plane (red or green plane), three out of every six atoms shuffle by 0.74 A along $[1\bar{2}10]$ and subsequently in the $[10\bar{1}0]$ direction with a magnitude 0.204 Å; the other three atoms shuffle in the opposite direction $[\bar{1}2\bar{1}0]$. This creates the $(1\bar{2}10)_\omega$ plane from $(0001)_\alpha$. Shuffle directions are opposite in successive planes. (For interpretation of the references to color in this figure legend, the reader is referred to the web version of this article.)

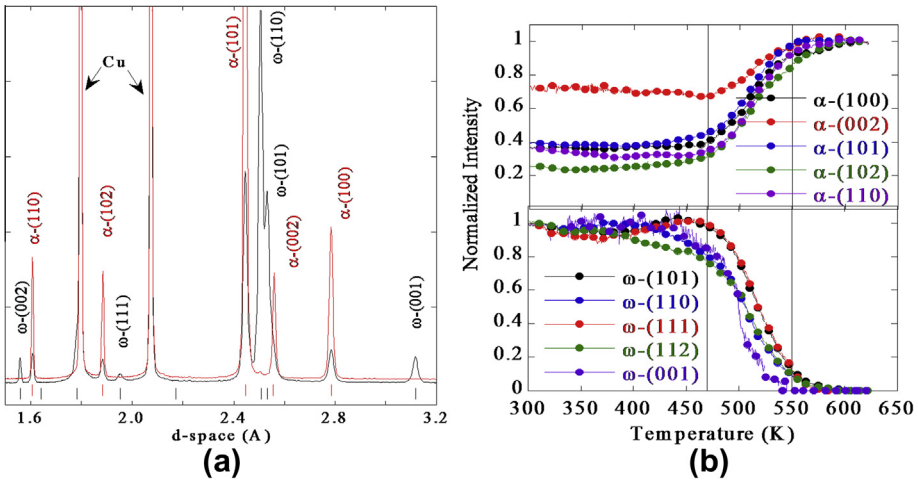

Fig. 5. (a) X-ray diffraction patterns collected from the sample shocked to 8 GPa peak pressure (black) and following subsequent anneal to 630 K (red). The black (ω) and red (α) tick marks indicate the expected diffraction peak locations. Several peaks from each phase are indexed. Copper peaks from the sample holder are also indicated. (b) Evolution of the normalized peak intensities of several peaks (hkl) from each phase in the sample during continuous heating at 3 K min^{-1} in the material shocked to 8 GPa (from Ref. [16]). (For interpretation of the references to color in this figure legend, the reader is referred to the web version of this article.)

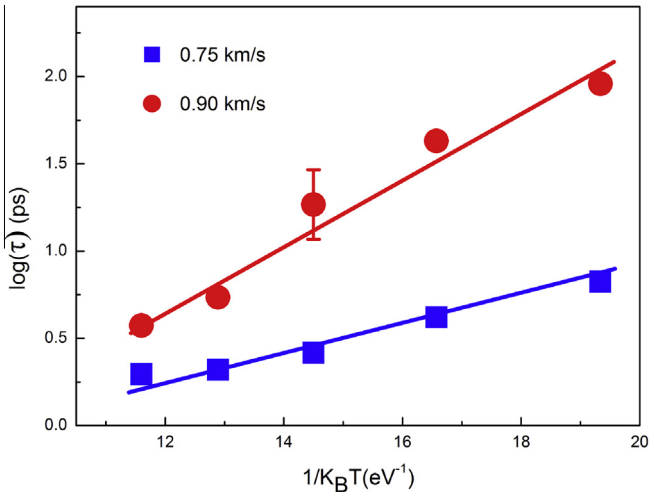

Fig. 6. The activation barriers for shocked Ti single crystals. The logarithm of relaxation time log(τ) vs. the inverse of absolute transformation temperature, $1/k_BT$, from the analysis of our MD simulation data for shock-recovered samples obtained using different piston velocities or peak pressures. The higher energy barrier to the reverse transformation for higher velocities or pressures follows the same trend as the Zr polycrystal annealing data.

[30–33]. In particular, the specific microscopic mechanisms responsible for the thermally activated nature of isothermal MT have not been elucidated. More recent experiments on the kinetics of MT seem to suggest a number of explanations for the activation energy for martensite formation: (i) Kurdjumov and Maksimova [34,35] analyzed experimental data using a model with a combination of nucleation and growth components. The low-temperature branch of the TTT curve is dominated by the activation energy for growth of a martensite embryo to its critical size from where spontaneous growth can occur; the activation energy for nucleation controls the high-temperature branch; (ii) according to the model developed by Pati and Cohen [36,37] and Cohen and Kaufman [38], the temperature-dependent activation energy can be explained as a direct result of extending the classical theory of fluctuation nucleation to martensitic transformations. In this model it is assumed that the transformation rate is controlled by the nucleation of new plates homogeneously or heterogeneously, rather than by the growth of existing ones; and (iii) recent experiments on shape memory alloys (such as NiTi) [2] strongly support the interpretation of the observed isothermal effects as being due to the interaction of solute atoms with the diffusionless but thermally assisted motion of the martensitic interface.

As mentioned above, the peak pressure of the shock compression influences the volume fraction of the retained ω phase and the crystal defects due to plastic deformation. In order to understand the microscopic mechanisms responsible for the differences in activation energies with peak stresses obtained from our X-ray data, we used atomistic simulations to study how the kinetics of the MT correlates with the volume fraction of ω phases, as well as the defect concentration. The initial samples were created by starting from pure α phase and converting a given volume fraction to the ω phase, ensuring the Silcock OR. The configuration is allowed to relax, as shown in Fig. 7. We designed three types of samples: two containing 60% and 80% volume fractions of ω phase, respectively, without any defects, and the third with a 2% volume fraction of point defects in a sample containing an 80% volume fraction of ω phase. At high temperatures, these samples will lead to a mixture of point defects and dislocations. The samples were annealed at given temperatures, and the volume fraction of ω was monitored as a function of time (Fig. 8). The relaxation data from the simulations were then fitted to Eq. (3).

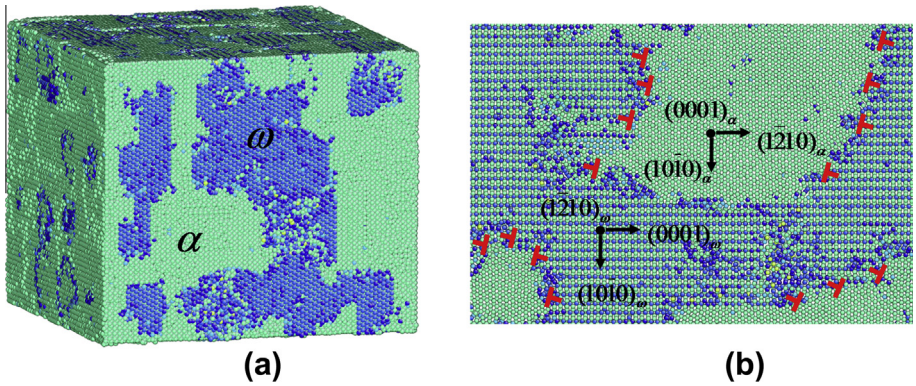

Fig. 7. Model microstructure with coexisting α and ω phases. (a) A configuration with 60% ω phase (stacked planes) in α matrix (green). (b) A cross-section of the sample in (a) showing the validity of the Silcock orientation relationship, consistent with our X-ray measurements. (For interpretation of the references to color in this figure legend, the reader is referred to the web version of this article.)

The $\log(\tau) \sim 1/T$ data for the three samples are shown in Fig. 9. The data for the 60% ω phase as well as the 80% ω phase shows that the activation energy increases with the volume fraction of the ω phase. It is consistent with our analysis of the shock experiments at 8.0 and 10.5 GPa. This result can be understood if we consider that the MT is dominated by the nucleation process, in which the martensite interface dislocations serve as the primary heterogeneous nucleation centers, as shown in Fig. 10(a). The area of the ω–α interface in the 80% ω phase volume fraction samples is expected to be smaller than in the 60% ω phase samples (Fig. 10(b)). Thus, nucleation is less probable for the 80% case than for the 60% case, and this explains the trend in the barrier estimates from our experimental and simulations results. It is analogous to surface-catalyzed reactions, in which a high specific surface area can accelerate the reaction rate. In order to further confirm our understanding, we compare the data of the 80% ω phase with and without the 2% defect in Fig. 9. We see that the ω → α transformation is accompanied by a decrease in activation energy and an increase in point defect concentration. For an MT, defects can act as either heterogeneous

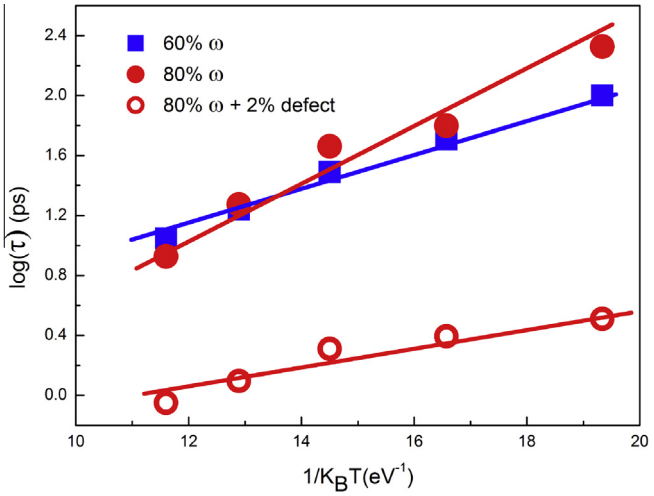

Fig. 9. The dependence of the activation barrier energy for different defect concentrations from our MD simulations. Shown are the logarithm of the relaxation time $\log(\tau)$ vs. the inverse of absolute transformation temperature, $1/k_BT$, for the microstructure of Ti with 60% ω phase (without defects) and 80% ω phase with 0% and 2% volume fractions of point defects. The presence of defects lowers the barrier and can increase the phase transformation rate.

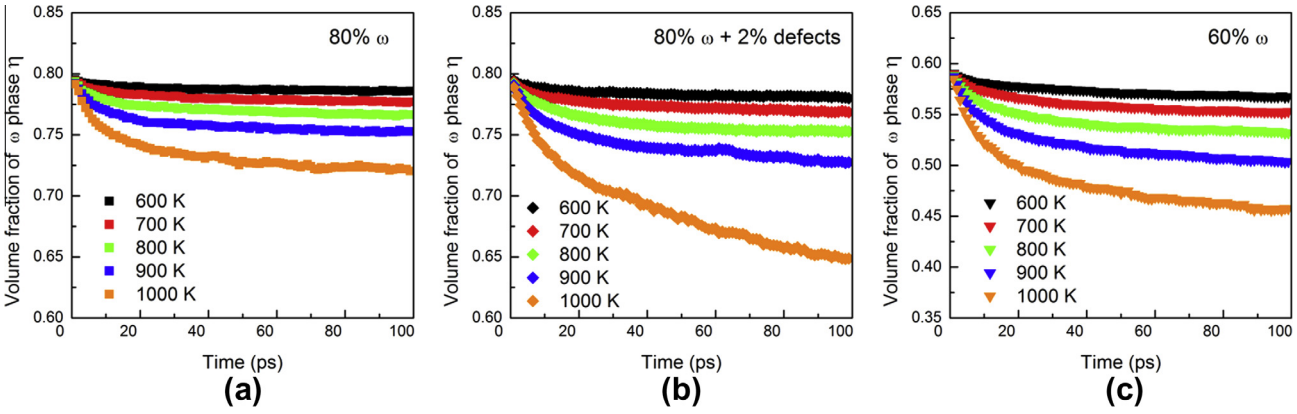

Fig. 8. MD simulation results for isothermal annealing showing the volume fraction of ω phase for different samples with varying volume fractions of ω and α phases and defects. (a) 80% ω phase without defects; (b) 80% ω phase with 2% defects; (c) 60% ω phase without defects.

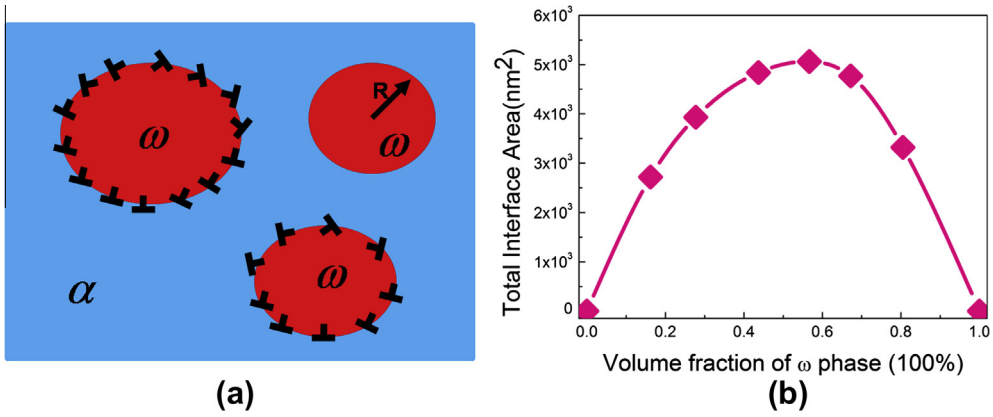

Fig. 10. (a) Schematic illustration of the heterogeneous nucleation model for the $\omega \rightarrow \alpha$ martensitic transformation (see Fig. 7(b)). (b) The relationship between the total interface area and the volume fraction of ω phase calculated from our MD simulations shows that the interface area peaks at roughly 58% volume fraction of ω phase.

nucleation centers or obstacles for the migration of the martensitic interfaces. From this point of view, the data of 80% ω phase in Fig. 9 indicates that the transformation is due to a nucleation- rather than growth-dominated process. Otherwise, the increasing interaction of defects with martensite interfaces will place strong constraints on the MT interface movement and significantly increase the activation energies, as occurs in the case of the isothermal MT in TiNi alloys [2]. Our work has parallels to the $\alpha \rightarrow \omega$ transformation in titanium under quasi-static pressure, where it has been shown that cold-worked samples have higher transformation rates than the annealed case [11]. The grain boundaries and defects assist critical nuclei formation, leading to a higher transformation rate for cold-worked samples due to their smaller grain size and higher dislocation densities.

Our results favor a process involving nucleation by defects (such as dislocations) rather than an interface migration-mediated growth of existing α phase. For the growth of the α phase embryos or domains, the mechanism is known to be the structural transformation of the region coupled with a collective glide of martensitic interface dislocations [39–41]. As a martensitic interface moves across in Fig. 11, it produces a transformation of the parent phase lattice (red region) into the structure of the growing or product phase (blue region). The essence of the coupling effect is that this lattice transformation is accompanied by a specific shape deformation or lattice-invariant shear of the swept region (yellow region), which involves the generation and migration of parallel interface dislocation arrays. Our previous studies have suggested that the ω phase constitutes a sluggish dislocation system in which the reverse phase transformation is energetically preferred [42]. The thermally assisted motion of the martensitic interface is thus less likely to occur than the defect-mediated heterogeneous nucleation process.

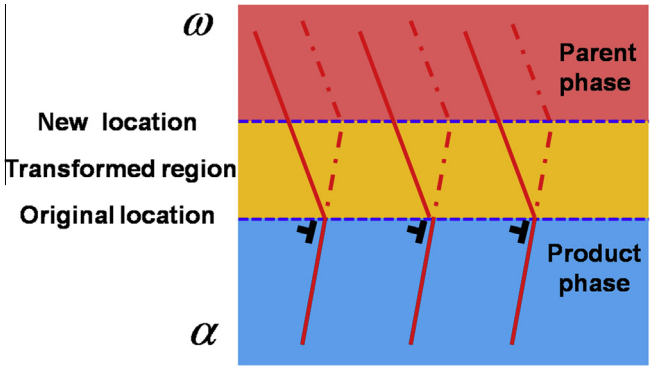

Fig. 11. Schematic illustration of the mechanism of $\omega \rightarrow \alpha$ phase boundary migration. For the dislocation-meditated phase boundary motion, the ability of the interface dislocations to glide determines the growth of new phase embryos for the $\omega \rightarrow \alpha$ phase transformation. The solid and dashed lines show selected atomic planes before and after the interface displacement, respectively.

4. Conclusions

We have studied the isothermal nature of the $\alpha \rightarrow \omega$ transformation using shocked polycrystal Zr microstructure combined with in situ X-ray diffraction measurements and large-scale MD simulations on Ti. Our main findings are as follows: (i) we fit a Kohlraush–Williams–Watts equation, together with thermal activation for the relaxation, to the in situ heating measurements for shocked microstructure. We show that the effective barrier activation energies to transformation increase with the peak pressure (10.5 or 8.0 GPa) or higher volume fraction of the ω phase in the microstructure; (ii) the OR for the reverse $\omega \rightarrow \alpha$ MT in the polycrystal data for Zr is consistent with the transformation pathway suggested by Silcock for Ti; and (iii) our MD simulation results for the microstructures with varying ω volume fractions and containing different concentrations of lattice defects, as well as our in situ data, show that transformation can be modeled as a thermally activated process resulting from heterogeneous nucleation.

Acknowledgments

This work was supported by US DOE at LANL (DE-AC52-06NA25396) and NSFC (51171140, 51231008, 51320105014 and 51321003), the 973 Program of China (2010CB631003, 2012CB619402) and the 111 project (B06325).

References

[1] Thadhani NN, Meyers MA. Prog Mater Sci 1986;30:1.
[2] Kustov S, Salas D, Cesari E, Santamarta R, Van Humbeeck J. Acta Mater 2012;60:2578.
[3] Shekar NVC, Rajan KG. Bull Mater Sci 2001;24:1.
[4] Kakeshita T, Takeguchi T, Fukuda T, Saburi T. Mater Trans JIM 1996;37:299.
[5] Borgenstam A, Hillert M. Acta Mater 2000;48:2777.
[6] Sikka SK, Vohra YK, Chidambaram R. Prog Mater Sci 1982;27:245.
[7] Singh AK, Mohan M, Divakar C. J Appl Phys 1983;54:5721.
[8] Dammak H, Dunlop A, Lesueur D. Philos Mag A 2000;80:501.
[9] Leyens C, Peters M. Titanium and titanium alloys: fundamentals and applications. Weinheim: Wiley-VCH; 2003.
[10] Singh AK. Bull Mater Sci 1983;5:219.
[11] Vohra YK. J Nucl Mater 1978;75:288.
[12] Silcock JM. Acta Metall 1958;6:481.
[13] Wenk HR, Kaercher P, Kanitpanyacharoen W, Zepeda-Alarcon E, Wang Y. Phys Rev Lett 2013;111:195701.
[14] Todaka Y, Sasaki J, Moto T, Urnernoto M. Scripta Mater 2008;59:615.
[15] Cerreta E, Gray Iii GT, Hixson RS, Rigg PA, Brown DW. Acta Mater 2005;53:1751.
[16] Brown DW, Almer JD, Balogh L, Cerreta EK, Clausen B, Escobedo-Diaz JP, et al. Acta Mater 2014;67:383.
[17] Cerreta EK, Escobedo JP, Rigg PA, Trujillo CP, Brown DW, Sisneros TA, et al. Acta Mater 2013;61:7712.
[18] Von Dreele RB. J Appl Cryst 1997;30:517–25.
[19] Zong H, Lookman T, Ding X, Luo S-N, Sun J. Acta Mater 2014;65:10.
[20] Hennig RG, Lenosky TJ, Trinkle DR, Rudin SP, Wilkins JW. Phys Rev B 2008;78:054121.
[21] Martyna GJ, Tobias DJ, Klein ML. J Chem Phys 1994;101:4177.
[22] Ackland GJ, Jones AP. Phys Rev B 2006;73:054104.
[23] Plimpton S. J Comput Phys 1995;117:1.
[24] Li J. Model Simul Mater Sci Eng 2003;11:173.
[25] Takano H, Nakanishi H, Miyashita S. Phys Rev B 1988;37:3716.
[26] Granzow T, Dörfler U, Woike T, Wöhlecke M, Pankrath R, Imlau M, et al. Phys Rev B 2001;63:174101.
[27] Ding X, Lookman T, Zhao Z, Saxena A, Sun J, Salje EKH. Phys Rev B 2013;87:094109.
[28] Lupascu DC, Fedosov S, Verdier C, Rodel J, von Seggern H. J Appl Phys 2004;95:1386.
[29] Trinkle DR, Hennig RG, Srinivasan SG, Hatch DM, Jones MD, Stokes HT, et al. Phys Rev Lett 2003;91:025701.
[30] Massalski TB. Mater Trans 2010;51:583.
[31] Kakeshita T, Kuroiwa K, Shimizu K, Ikeda T, Yamagishi A, Date M. Mater Trans JIM 1993;34:423.
[32] Perez-Reche FJ, Vives E, Manosa L, Planes A. Phys Rev Lett 2001;87:195701.
[33] Kurdjumov GV. J Iron Steel Inst 1965;195:26.
[34] Kurdjumov GV, Maksimova OP. Dokl Akad Nauk SSSR 1948;61:83.
[35] Kurdjumov GV, Maksimova OP. Dokl Akad Nauk SSSR 1950;73:95.
[36] Pati SR, Cohen M. Acta Metall 1969;17:189.
[37] Pati SR, Cohen M. Acta Metall 1971;19:1327.
[38] Kaufman L, Cohen M. Prog Metal Phys 1958;7:165.
[39] Bilby BA. Prog Solid Mech 1960;1:329.
[40] Hirth JP, Pond RC, Hoagland RG, Liu XY, Wang J. Prog Mater Sci 2013;58:749.
[41] Christian JW. The theory of transformations in metals and alloys. Oxford: Pergamon Press; 2002.
[42] Zong H, Ding XD, Lookman T. Unpublished data.